Electronic Supplementary Material (ESI) for Nanoscale.

Supplementary Information

Study of the nucleation and growth of antibiotic labeled Au NPs and blue luminescent Au_8 quantum clusters for Hg^{2+} ion sensing, cellular imaging and antibacterial applications

Puneet Khandelwal[1,2], Dheeraj K. Singh[1,2], Subha Sadhu[1,2], Pankaj Poddar*[1,2,3]

[1]Physical & Material Chemistry Division, CSIR-National Chemical Laboratory, Pune – 411008, India, [2]Academy of Scientific and Innovative Research, Anusandhan Bhawan, 2 Rafi Marg, New Delhi-110 001, [3]Center of Excellence on Surface Science, CSIR-National Chemical Laboratory, Pune – 411008, India

Dynamic light scattering (DLS) study

The dynamic light scattering measurements were performed to analyze the hydrodynamic diameter of the particles synthesized at different pH in solution phase, globally. We have shown the results, both in the form of particle numbers and intensity because the intensity (I) depends on the particle diameter (d) by d^6 by following equation:

$$I = I_0 \left[\frac{1+cos^2\theta}{2R^2}\right](2\pi/\lambda)^4 \left[\frac{n^2-1}{n^2+1}\right]^2 \left[\frac{d}{2}\right]^6$$

And, therefore, the contribution in the intensity by big particle will be very large and that will neglect the contribution from even a big population of small size particles.

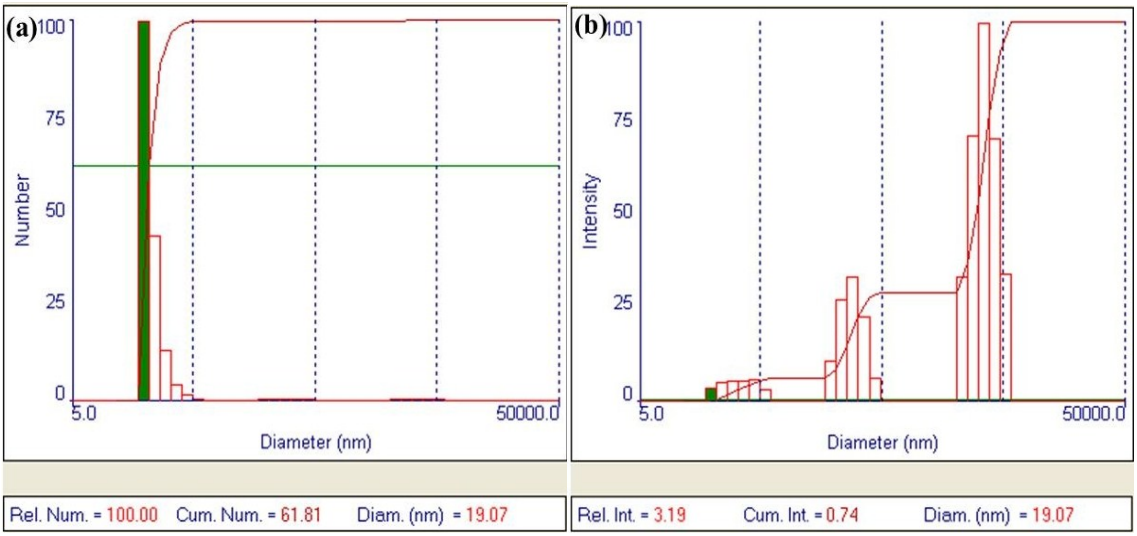

Figure S1. Dynamic light scattering measurements (a) particle numbers and (b) intensity of scattering light, of gold nanoparticle suspension synthesized at pH 4. The study shows the presence of a large population of ca. 19 - 50 nm particles with a small population of big nanoparticles and large aggregates.

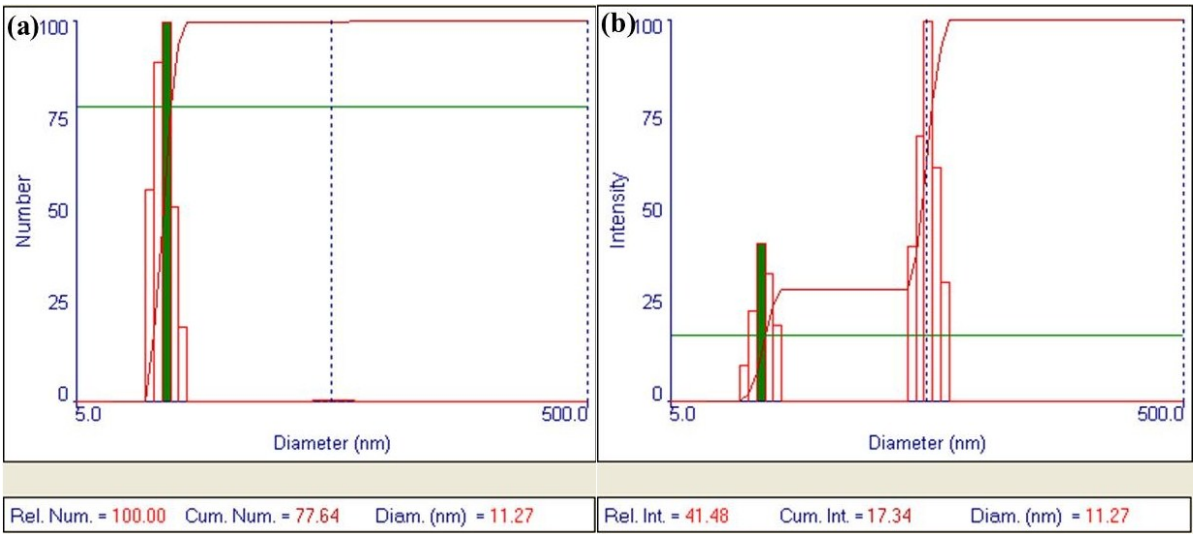

Figure S2. Dynamic light scattering measurements (a) particle numbers and (b) intensity of scattering light, of gold nanoparticle suspension synthesized at pH 5. The study shows the presence of a large population of ca. 9 - 13 nm particles with a small population of big nanoparticles and small aggregates (ca. 50 nm).

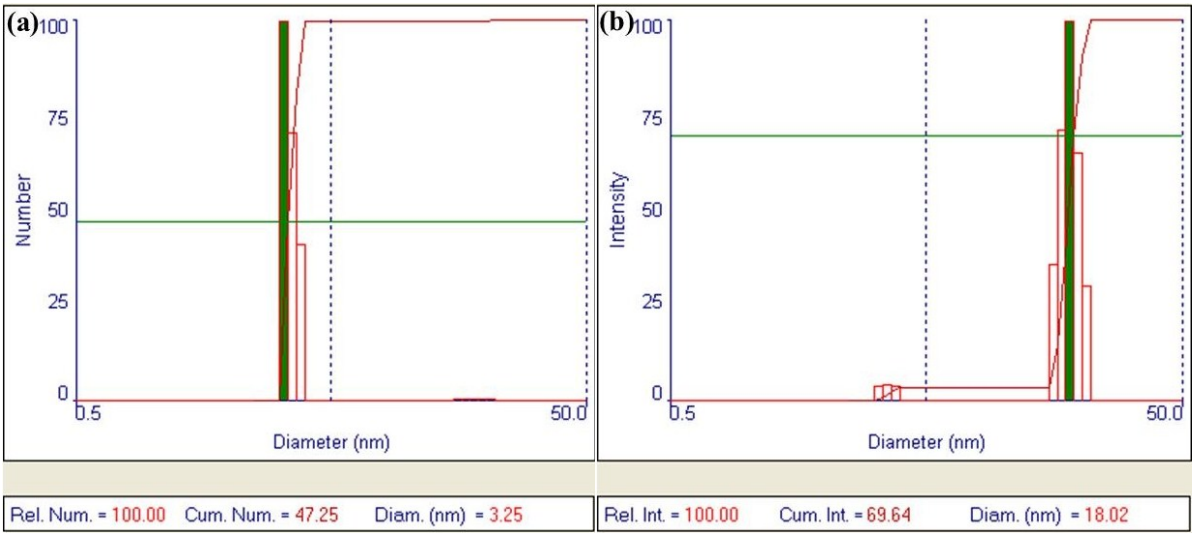

Figure S3. Dynamic light scattering measurements (a) particle numbers and (b) intensity of scattering light, of gold nanoparticle suspension synthesized at pH 6. The study shows the presence of a large population of ca. 3 - 4 nm particles with a small population of big nanoparticles and small aggregates (ca. 18 nm).

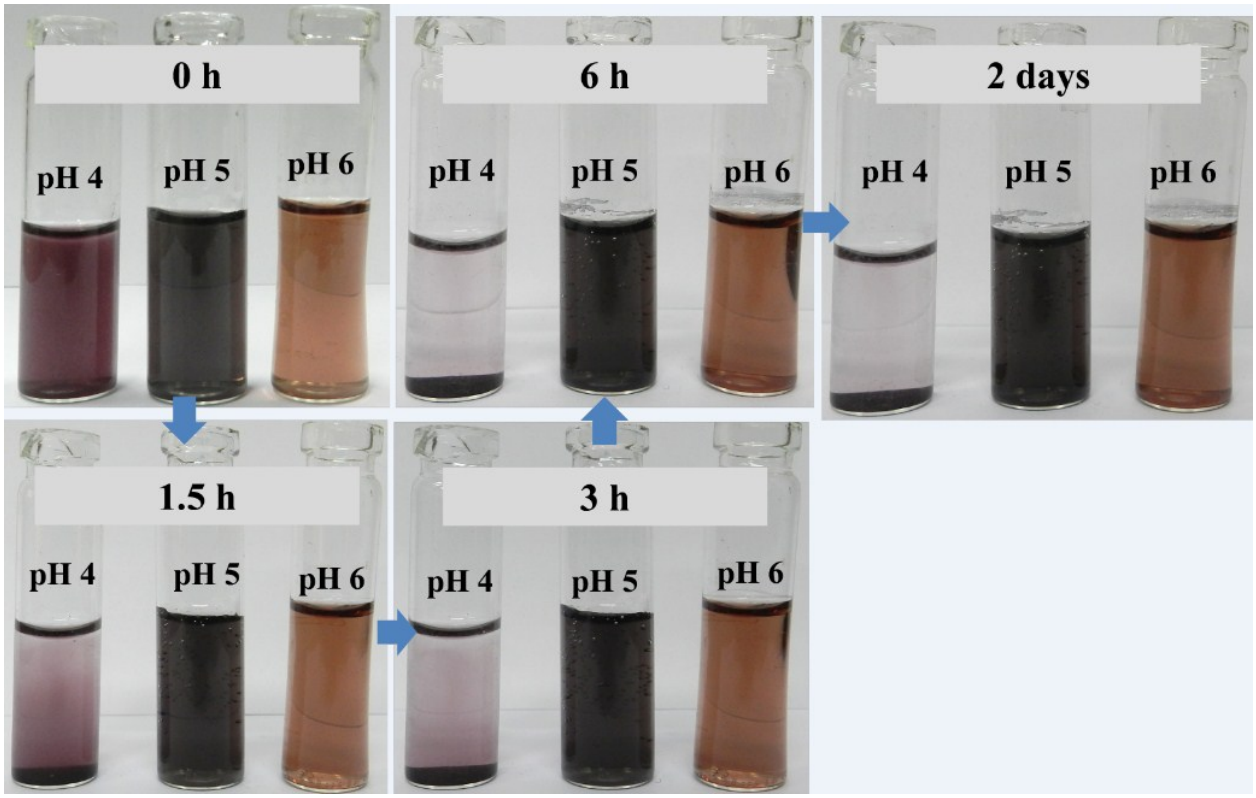

Figure S4. Photographs of reaction suspension synthesized at pH 4, pH 5 and pH 6 at different time period showing the stability of the suspensions.

Powder X-ray diffraction (PXRD) study

The change in the crystalline structure of the synthesized CFD labeled Au NPs at different concentration of $HAuCl_4$ (10^{-3} M to 10^{-4} M), temperature (10 ^oC to 50 ^oC) and pH (4 to 6) of the reaction (where the final concentration of both the constituents (CFD and $HAuCl_4$) was 5×10^{-4} M and reaction temperature was 27 ^oC), was studied through PXRD and presented in figures S5a, b and c, respectively. The presence of peaks at 2θ = 38.2, 44.3, 64.5, and 77.6° in figures S5a, b and c corresponding to the (111), (200), (220), and (311) planes were in good agreement with the standard data. The peaks which are mentioned with asterisk might be because of the antibiotic crystallization. The XRD pattern revealed the relative dominance of (111) plane when the Au NPs synthesized at higher $HAuCl_4$ concentrations, decrease in the temperature and decrease in pH of the reaction indicating the increase in the synthesis of anisotropic nanostructures. The major difference was observed when the reaction was performed at different concentration of $HAuCl_4$. A comparison of (111) and (200) plane intensities show the increase in the relative intensity from 2.4 (for standard data) to 6 (when the both $HAuCl_4$ and CFD concentration was 5 X 10^{-4} M) and 17 (when the $HAuCl_4$ and CFD concentration was 10^{-3} M and 5 X 10^{-4} M, respectively) which suggests the dominance of (111) plane in as-synthesized CFD labeled Au NPs.

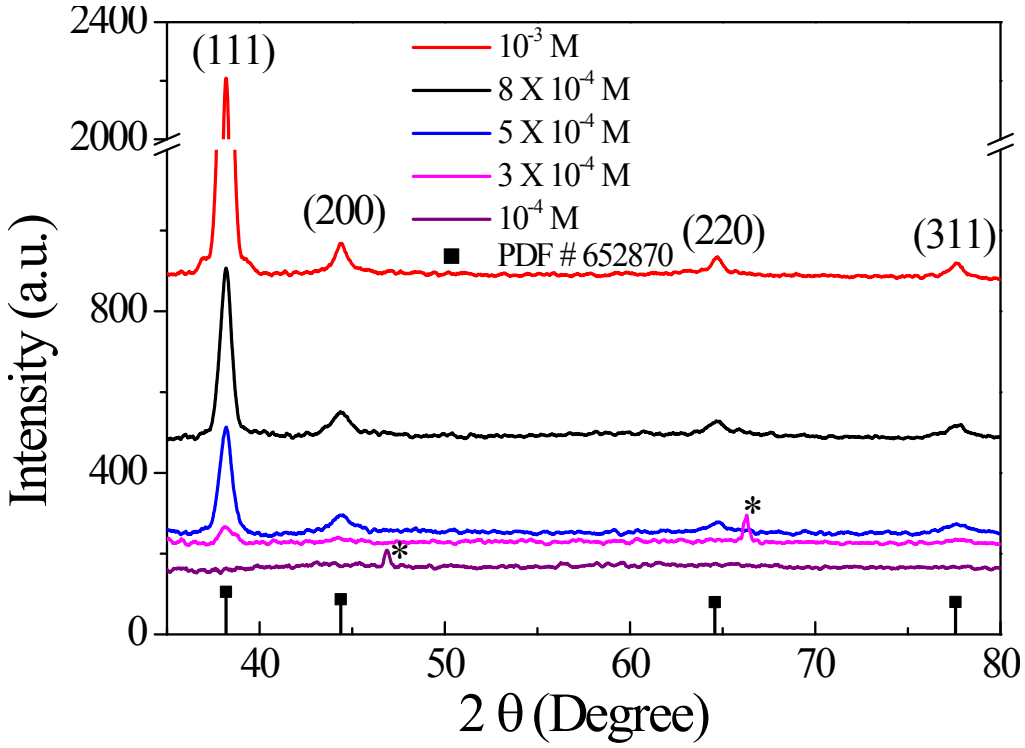

Figure S5a. Powder X-ray diffraction pattern of CFD labeled Au NPs synthesized at different concentrations of $HAuCl_4$. The data is compared with the standard data file # 652870.

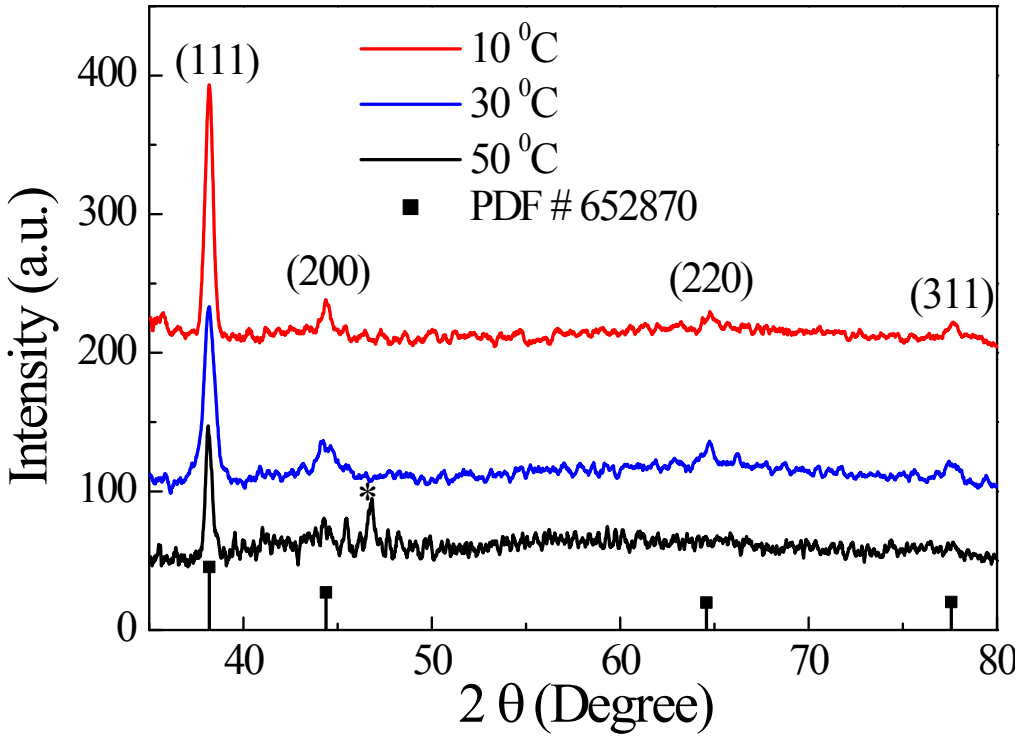

Figure S5b. Powder X-ray diffraction pattern of CFD labeled Au NPs synthesized at different temperatures at final concentration of 5×10^{-4} M for both CFD and $HAuCl_4$. The data is compared with the standard data file # 652870.

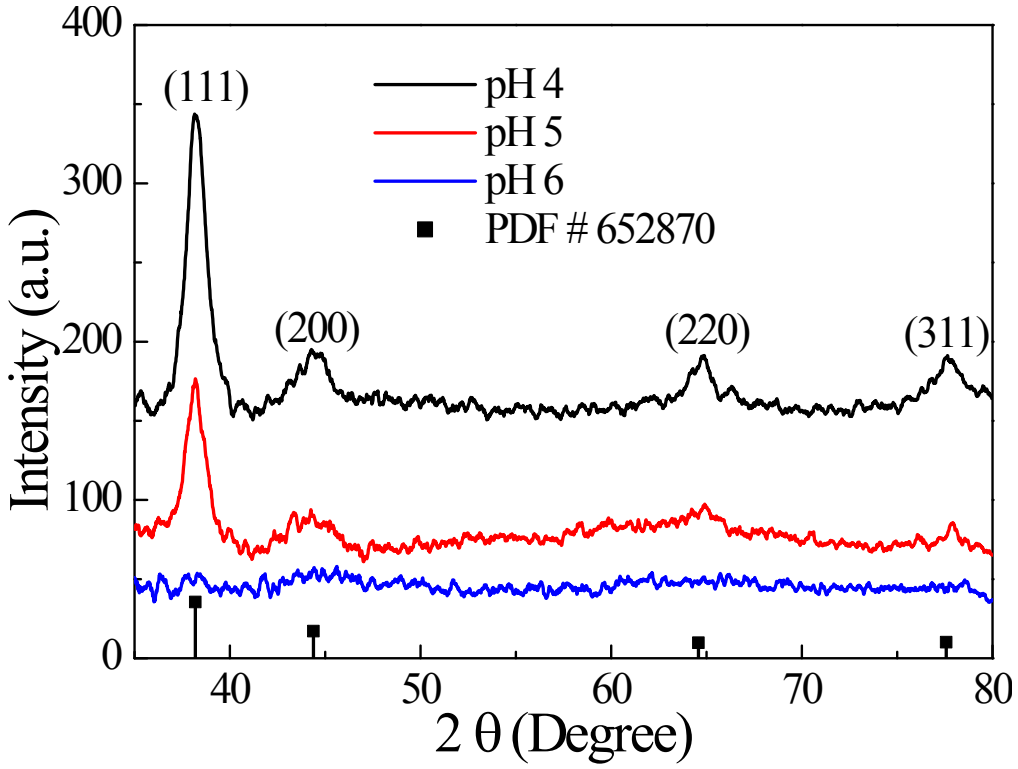

Figure S5c. Powder X-ray diffraction pattern of CFD labeled Au NPs synthesized at different reaction pH at final concentration of 5×10^{-4} M for both CFD and $HAuCl_4$. The data is compared with the standard data file # 652870.

FT-IR spectroscopic study

FT-IR spectra of aqueous solution of CFD and CFD labeled Au NPs [synthesized in a typical reaction where the final concentration of both constituents (CFD and $HAuCl_4$) were 5×10^{-4} M] have been presented in the Figure S6. CFD labeled Au NPs spectrum shows the broadening and damping of peaks in comparison with CFD aqueous solution spectrum, indicates the binding of CFD with Au NPs surface. A comparison of FTIR spectra of CFD and CFD labeled Au NPs show the down-shift of 1420 cm^{-1} (due to >C=O bond vibrations in the –N-C=O moiety) and 1751 cm^{-1} (due to >C=O bond vibrations of β-lactam ring) peaks in the CFD labeled Au NPs spectrum by ca. 20 and 16 cm^{-1}, respectively and indicates the involvement of >C=O group of β-lactam ring in the binding of CFD with Au NPs surface.

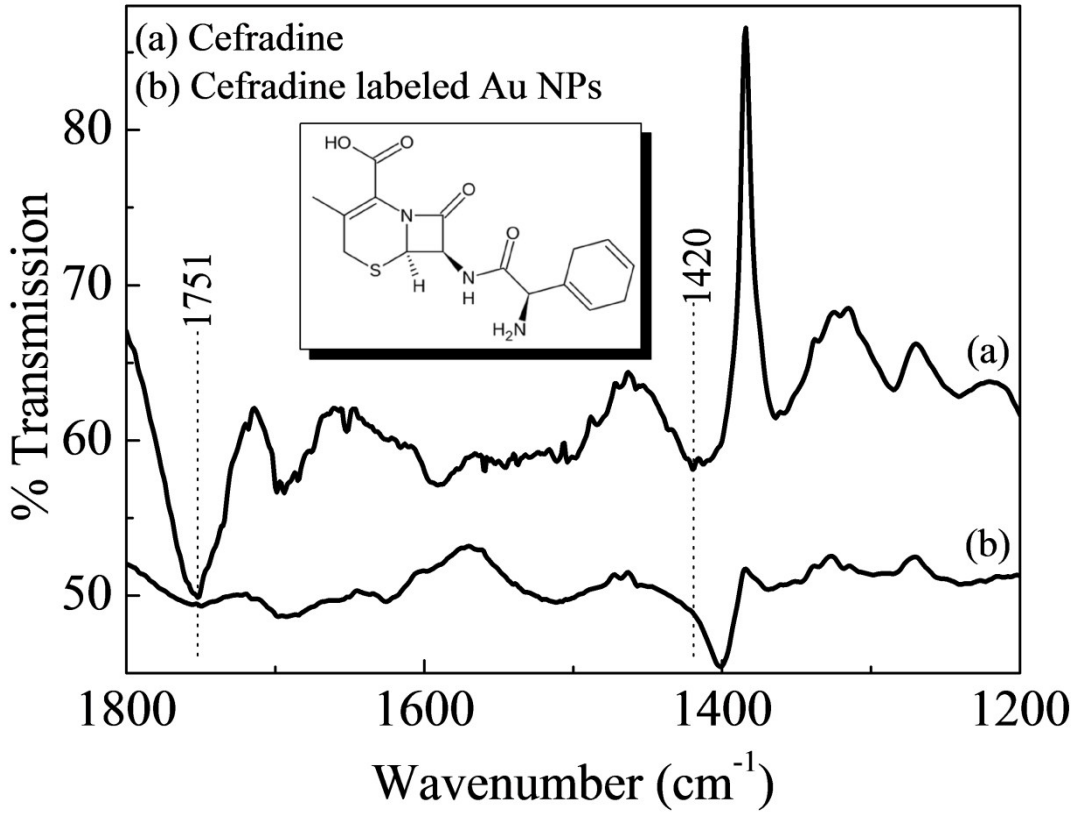

Figure S6. FTIR spectra of (a) 5×10^{-4} M CFD aqueous solution and (b) CFD labeled Au NPs synthesized at final concentration of 5×10^{-4} M for both CFD and $HAuCl_4$.

Raman spectroscopic study

In order to precisely determine the functional groups responsible in the surface capping of Au NPs, Raman spectra of CFD aqueous solution and CFD labeled Au NPs (synthesized at equimolar concentration of CFD and $HAuCl_4$, 5×10^{-4} M) were also recorded in the region 400-2000 cm^{-1} and presented in the Figure S7. The sharp and intense Stokes Raman shift peaks were observed at ca. 432, 710, 1265, 1388, 1655, 1703 and 1767 cm^{-1}, in the case of CFD aqueous solution. Only 1265 and 1767 cm^{-1} vibrational bands show blue shift of ca. 3 and 5 cm^{-1}, respectively, upon conjugation with Au NPs surface and these modes were assigned by Gauss View 03 software as the N-H_2 bending with mix vibration and ν(C=O) symmetric stretching vibration of β-lactam ring, respectively. The significant blue-shift of these two bands clearly indicate the involvement of N-H_2 group and >C=O group of β-lactam ring for surface passivation of the Au NPs surface. The sulfur moieties also play very crucial role for reduction/binding to Au NPs surface, however, in the Raman spectrum of CFD labeled Au NPs, it was not observed due to its low lying vibrational mode below 200 cm^{-1}. A comparison between Raman spectrum for CFD aqueous solution and CFD labeled Au NPs shows the enhancement of amine group peak intensity for CFD labeled Au NPs indicates the involvement of Surface Enhanced Raman Scattering (SERS) effect. However, it seems that the electromagnetic enhancement did not play any role in this case and the SERS in the amine group was due to only chemical enhancement via charge transfer mechanism.

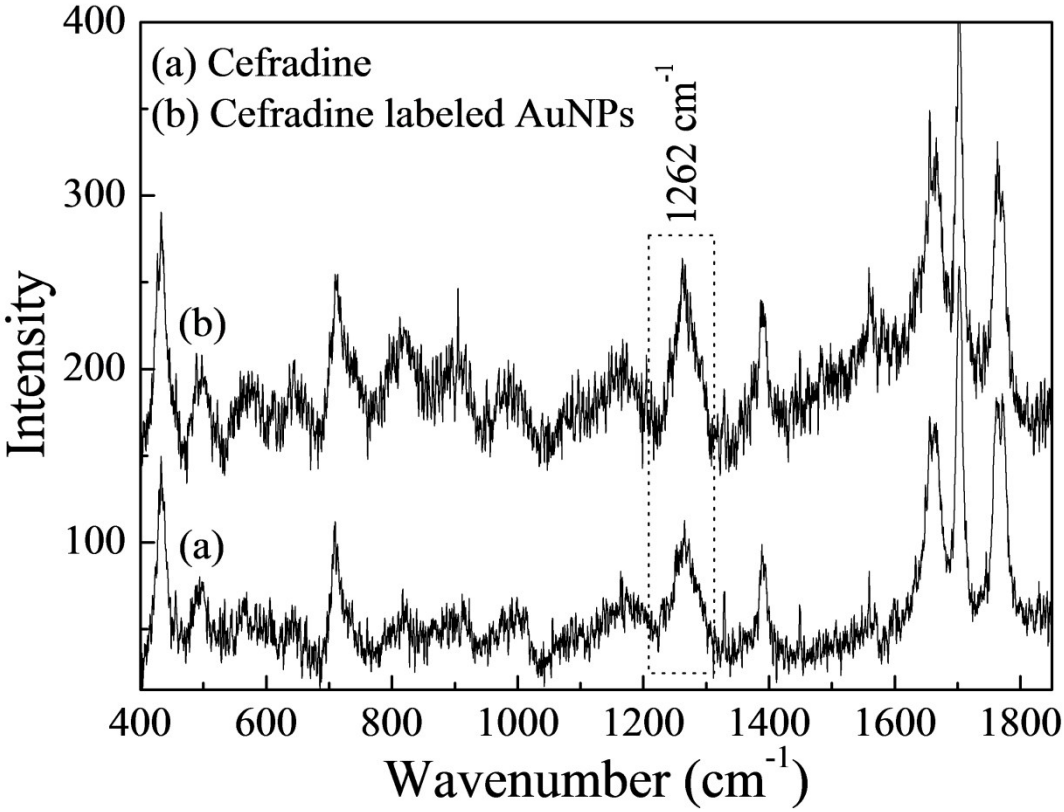

Figure S7. Raman spectra of 5×10^{-4} M aqueous solution of CFD and CFD labeled Au NPs (synthesized at final concentration of 5×10^{-4} M for both CFD and $HAuCl_4$ aqueous solutions).

XPS studies

Further chemical analysis of CFD labeled Au NPs was performed by XPS and compared with the XPS spectra of CFD. The results are presented in figure S8, where the panels in the left column (a-c) represent spectra for C 1*s*, N 1*s*, O 1*s* obtained from CFD alone, whereas, panels in the right column (d-g) show spectra corresponding to C 1*s*, N 1*s*, O 1*s*, and Au 4*f* core levels obtained from CFD labeled Au NPs. As-obtained XPS core level spectra were background corrected using the Shirley algorithm and chemically distinct species were resolved using a nonlinear least-square fitting procedure. The core level binding energies (B.E.) were aligned with the carbon B.E. of ca. 285 eV. As clear from figures S8a and d, the C 1*s* core level spectra could be resolved into three components situated at ca. 285, 286.6 and 288.2 eV B.E. Here, the peak at ca. 285 eV is due to electrons from saturated hydrocarbons, whereas the peaks at ca. 286.5 and 288.6 eV can be assigned to –COOH groups and α-carbon bound to -COOH and -NH_2 groups present in the CFD molecule, respectively. In figure S8b, N 1*s* core level spectra of CFD molecule has been plotted which shows two peaks at ca. 399.9 and 401.7 eV, due to two different N atoms in the CFD molecule with different electronic environments. These peaks were shifted to ca. 402.3 and 404.1 eV in the N 1*s* core level spectra of CFD labeled Au NPs. It was very significant shift (ca. 2.4 eV) in the B.E.'s corresponding to N 1*s* core level spectra of CFD labeled Au NPs, thus, it can be concluded that nitrogen is responsible for binding with the Au NPs in the present case. These results obtained from the N 1*s* core level spectra are consistent with FTIR and Raman spectroscopic data. Figures S8c and f show the spectra from the O 1*s* core level for CFD and CFD labeled Au NPs, situated at ca. 531.6 eV and 532.3 eV, respectively, with 0.7 eV shift which indicates that after the reaction the electronic environment of O atoms in the CFD molecule is slightly changed. In Figure S8g, the Au 4*f* core level spectrum has been presented which shows two peaks situated at ca. 84.2 and 87.9 eV. The peaks at ca. 84.2 and 87.9 eV are

attributed to $4f_{7/2}$ and $4f_{5/2}$, respectively, from Au^{o} state. Thus, XPS results clearly indicate that the amine and carbonyl group of (probably, β-lactam ring) CFD molecule simultaneously plays important role in binding to Au NPs surface, however, nitrogen moiety dominates over the oxygen moieties.

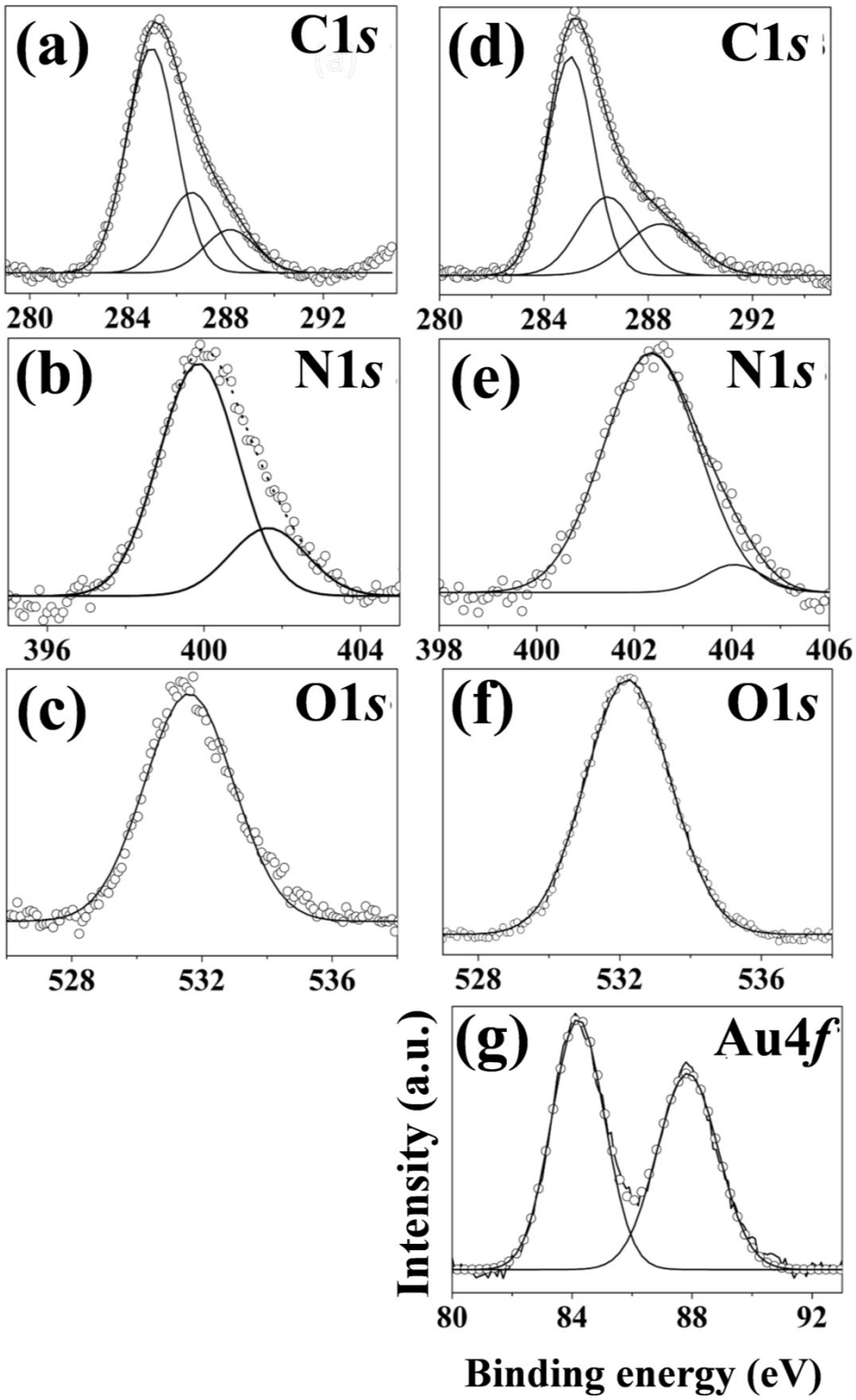

Figure S8. X-ray photoelectron spectroscopy data for 5×10^{-4} M CFD (panels, a-d) and CFD labeled Au NPs synthesized at final concentration of 5×10^{-4} M for both $HAuCl_4$ and CFD (panels, e-i).

DFT studies:

The CFD molecule has the sulfur, carbonyl and amine groups (as shown in Figure S9a) which may exist either as a monomer or different dimeric forms through intermolecular hydrogen bonds. By comparing the calculated energies of the CFD monomers to that of the dimeric species obtained by full geometric optimization, from our DFT results, it becomes quite evident that the dimer structures are more stable than the corresponding isolated monomers. Thus, the CFD molecules are expected to exist as a mixture of monomeric and dimeric species. For the first time, we conducted the DFT calculations on this molecule, which show three different possible dimeric forms of CFD, stabilized through hydrogen bonds (Figure S9 c, d, and e, respectively). Out of these three possible dimeric forms, we found on the basis of calculated optimized energies, binding energies and strength of hydrogen bonds that the dimer 3 appears to be most stable form (see Table S1).

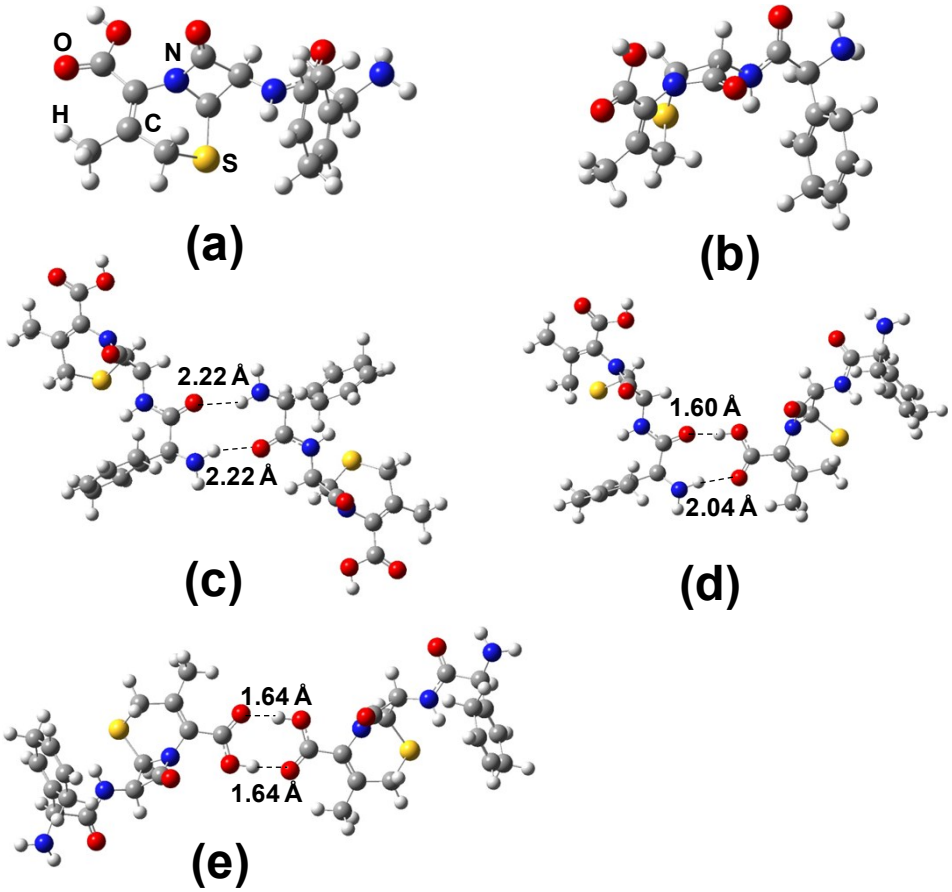

Figure S9: Optimized structures of CFD monomer in gas phase (different views, a, and b) and in various dimeric forms (c, d, and e). [Gray, white, red, blue and yellow colors indicate carbon, hydrogen, oxygen, nitrogen, and sulphur atoms, respectively].

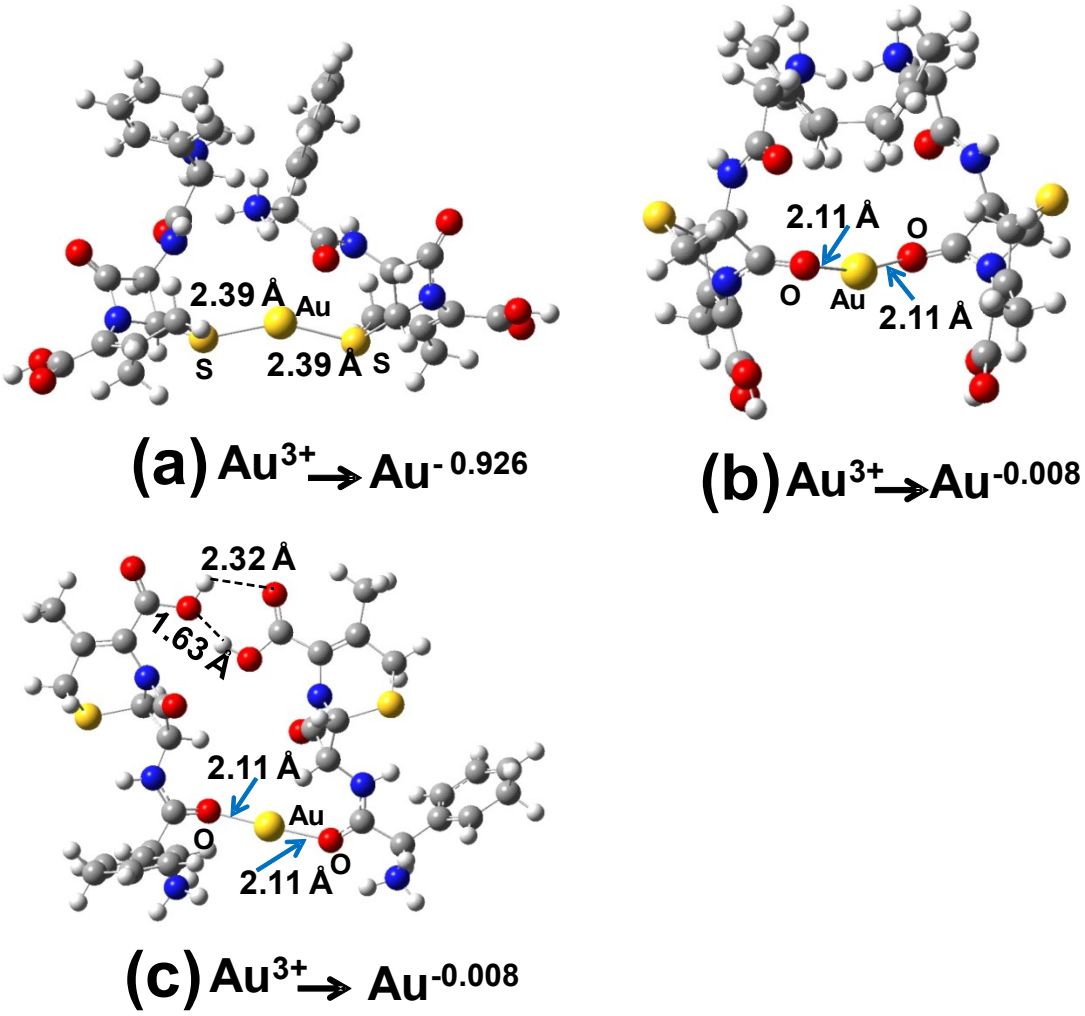

Figure S10: Optimized interactions of dimers of CFD with single Au^{3+} ion in different possible geometrical forms in aqueous environment using PCM approach (a) 2 CFD + 1 Au_1, (b) 2 CFD + 1 Au_3, (c) 2 CFD + 1 Au_4. [Gray, white, red, blue and yellow colors indicate carbon, hydrogen, oxygen, nitrogen, and sulphur atoms, respectively and the position of Au^{3+} ions is indicated separately in the figure.]

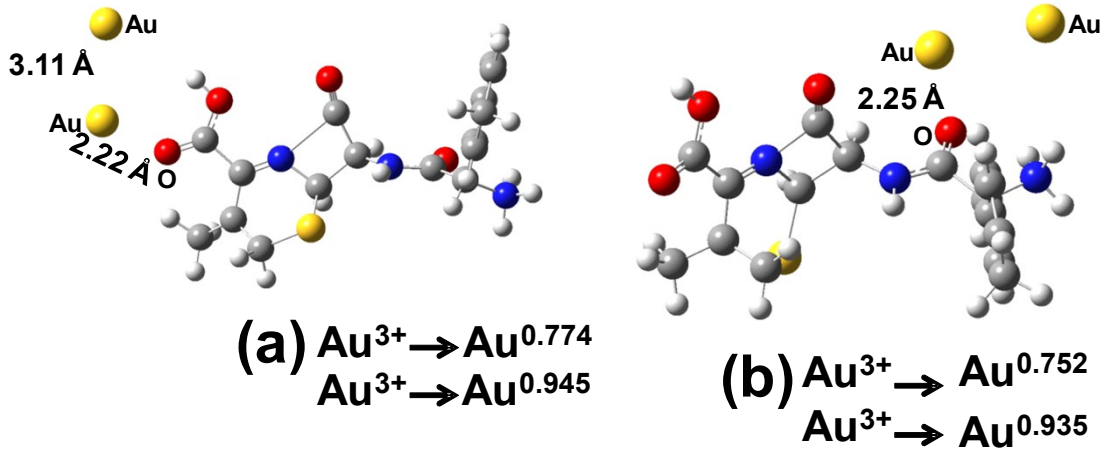

Figure S11: Optimized interactions of CFD monomer with Au^{3+} ions in aqueous environment using PCM approach (a) CFD + 2 Au_2, (b) CFD + 2 Au_4. [Gray, white, red, blue and yellow colors indicate carbon, hydrogen, oxygen, nitrogen, and sulphur atoms, respectively and the position of Au^{3+} ions is indicated separately in the figure.]

Electrostatic Potential (ESP) Mapping.

In order to validate and to understand the reducing property of CFD, we performed the molecular electrostatic potential (ESP) mapping. The molecular electrostatic potential (ESP) at a point *r* in the space around a molecule is given by (in atomic units):

$$V(r) = \sum \frac{Z_A}{|R_A - r|} - \int \frac{\rho(r)dr'}{|r' - r|} \quad (1)$$

where Z_A is the charge on nucleus A located at R_A and $\rho(r')$ is the electronic density. The first term in the expression represents the effect of the nuclei and the second represents that of electrons. Electrostatic potential correlates with dipole moment, electro-negativity, partial charges, and site of chemical reactivity of the molecule. It provides a visual method to understand the relative polarity of a molecule.

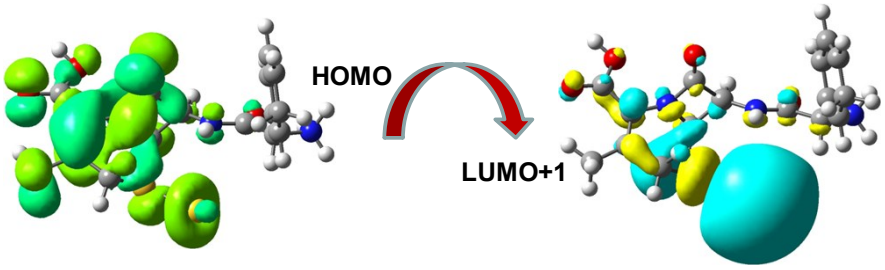

Figure S12: Highest occupied molecular orbital (HOMO) and lowest unoccupied molecular orbital (LUMO) level frontier orbital contour of CFD+1Au_1, complex using PCM having water environment which show the HOMO→LUMO + 1 electronic transition, an isosurface value of 0.02 e/Å^3 was used for orbital.

Table S1: Total electronic energies (E), binding energies (BE) and input - output charges for complexes of CFD with Au^{3+} ions

	E (a.u.)	BE (eV)	Charge (Au) (Input)	Charge (Au) (Output)
CFD	-1484.7883	-----	-----	-----
Dimer1	-2969.5810	00.12	-----	-----
Dimer2	-2969.5868	00.28	-----	-----
Dimer3	-2969.6007	00.66	-----	-----
CFD+1Au_1	-1619.7409	52.78	+3	-0.015
CFD+1Au_2	-1619.7168	52.12	+3	+0.628
CFD+1Au_3	-1619.7170	52.14	+3	+0.580
CFD+1Au_5	-1619.6252	49.63	+3	+0.867
2CFD+1Au_1	-3104.5413	53.11	+3	-0.926
2CFD+1Au_3	-3104.5836	54.26	+3	-0.008
2CFD+1Au_4	-3104.3397	47.62	+3	+0.015
CFD+2Au_1	-1754.4480	98.87	+6	+1.158
CFD+2Au_2	-1754.4380	98.60	+6	+1.719
CFD+2Au_4	-1754.4470	98.84	+6	+1.687
CFD+3Au_1	-1888.9979	140.69	+9	+3.566
CFD+3Au_5	-1888.9941	140.59	+9	+3.477

E (Au^{3+}) = -133.0130 a.u.

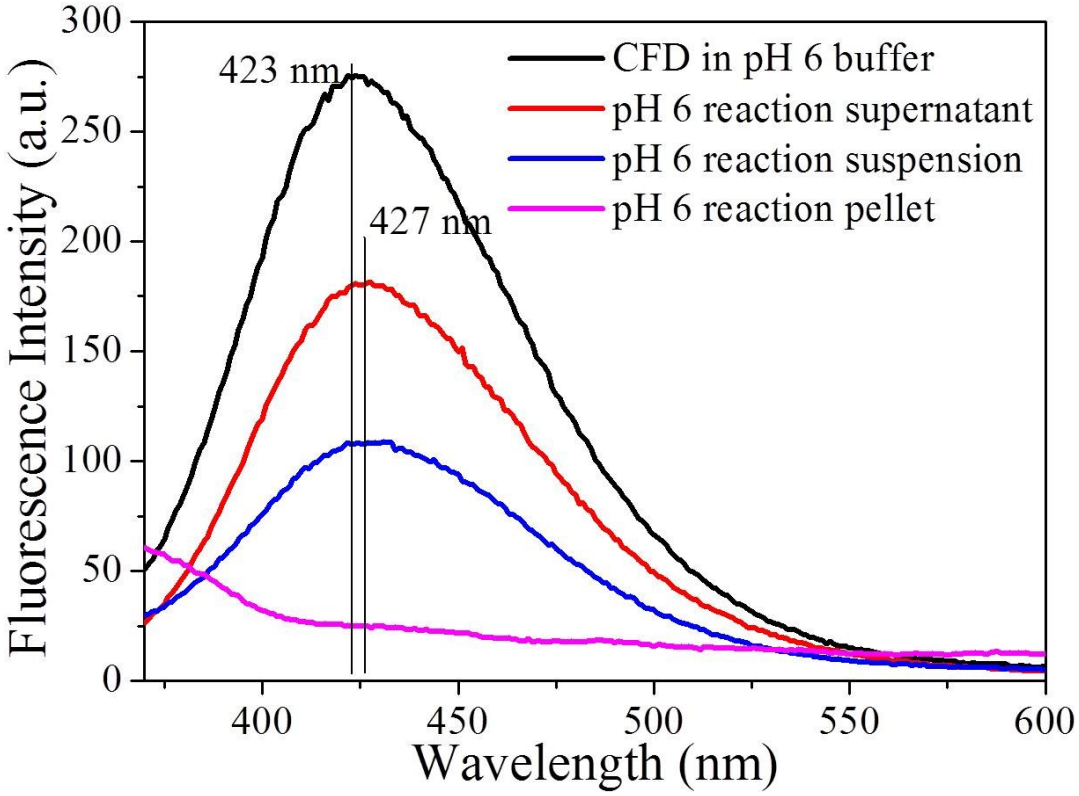

Figure S13. Fluorescence spectra of CFD in pH 6 buffer (black color), pH 6 reaction supernatant (red color), pH 6 reaction suspension (blue color), and pH 6 reaction pellet (magenta color) showing that with respect to CFD alone, fluorescence signal has red shifted by ca. 4 nm in case of Au QCs. It can also be seen that the fluorescence is very strong for Au QCs (supernatant), in comparison to the mixture of Au NPs and Au QCs (reaction suspension), and Au NPs alone (pellet).

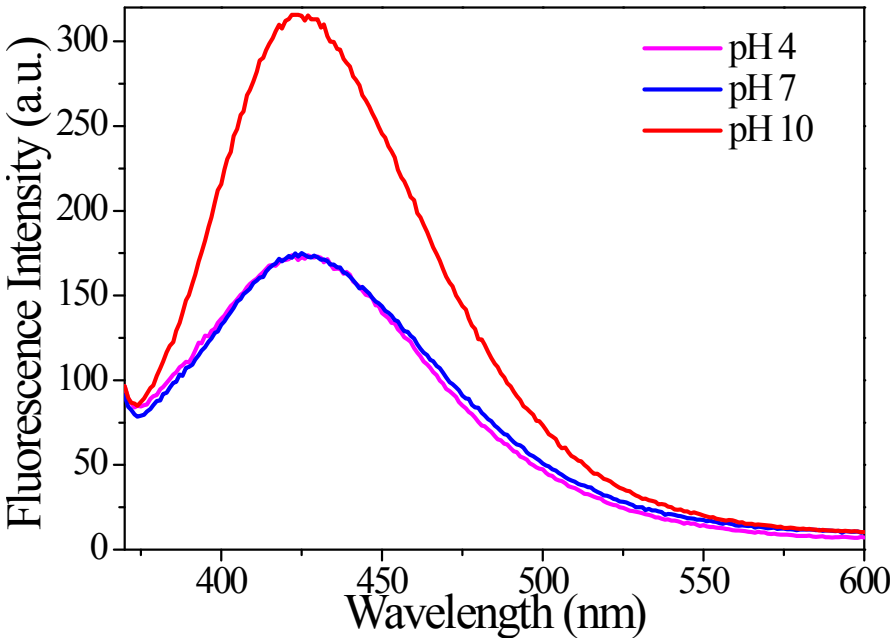

Figure S14. Fluorescence spectra of Au QCs as a function of change in the pH of the medium.

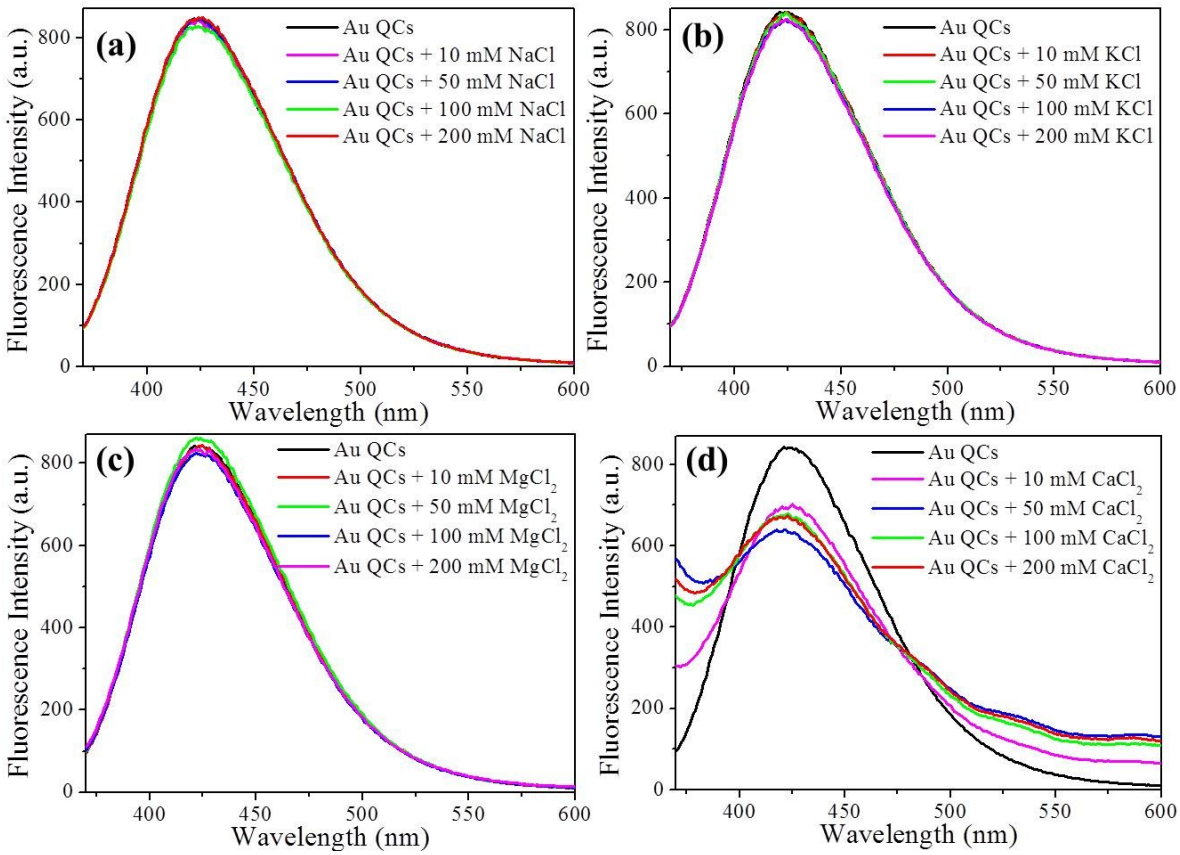

Figure S15. Fluorescence spectra of Au QCs in presence of (a) NaCl, (b) KCl, (c) $MgCl_2$, and (d) $CaCl_2$ salts at a concentration ranging from 0.01 M to 0.2 M. The decrease in the fluorescence in case of $CaCl_2$ may be due to the insolubility of $CaCl_2$ in pH 7 buffer.

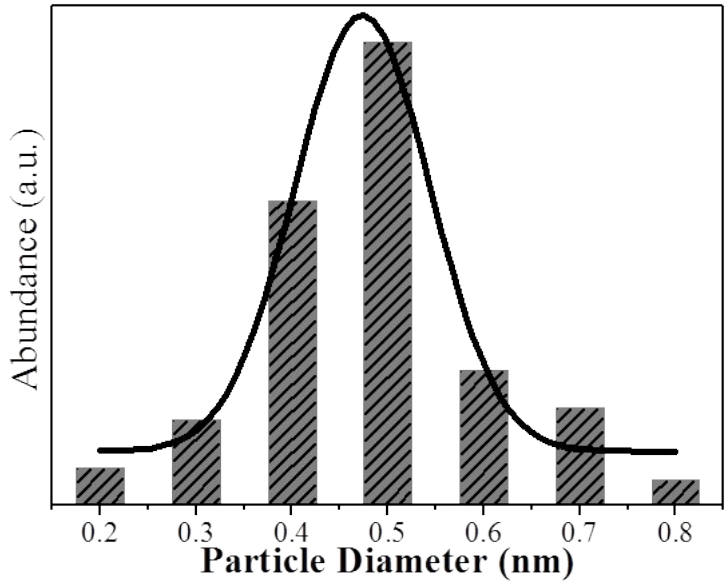

Figure S16. The population distribution histogram showing the particle size distribution in the Au QCs sample. The average size of the particles was found ca. 0.5 nm.

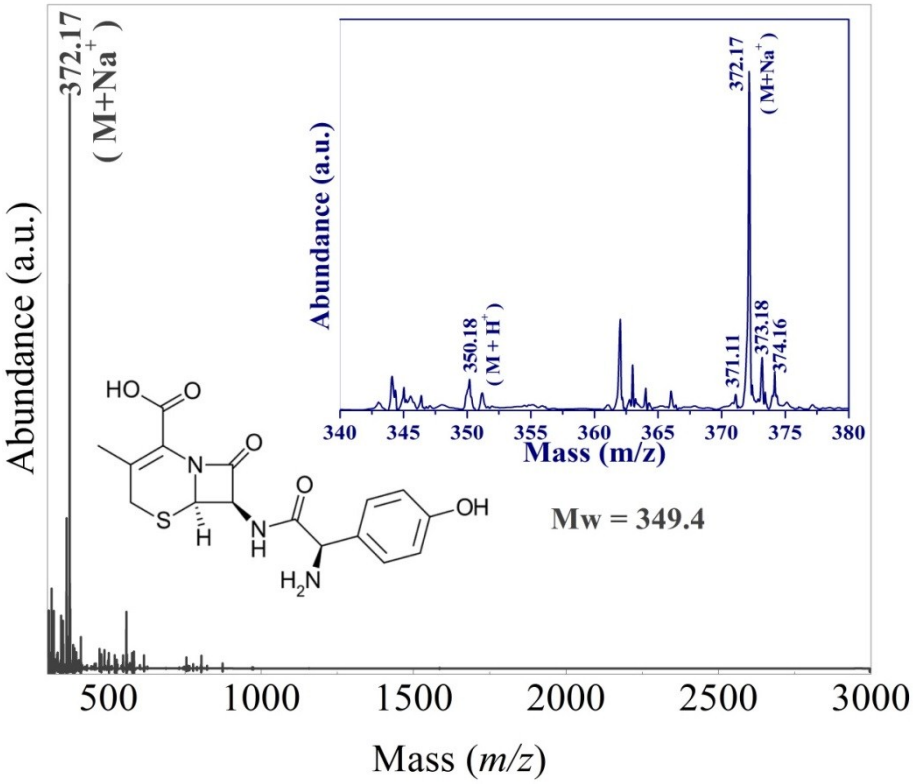

Figure S17. Positive ion mass spectrum for CFD aqueous solution. Inset shows the expanded view.

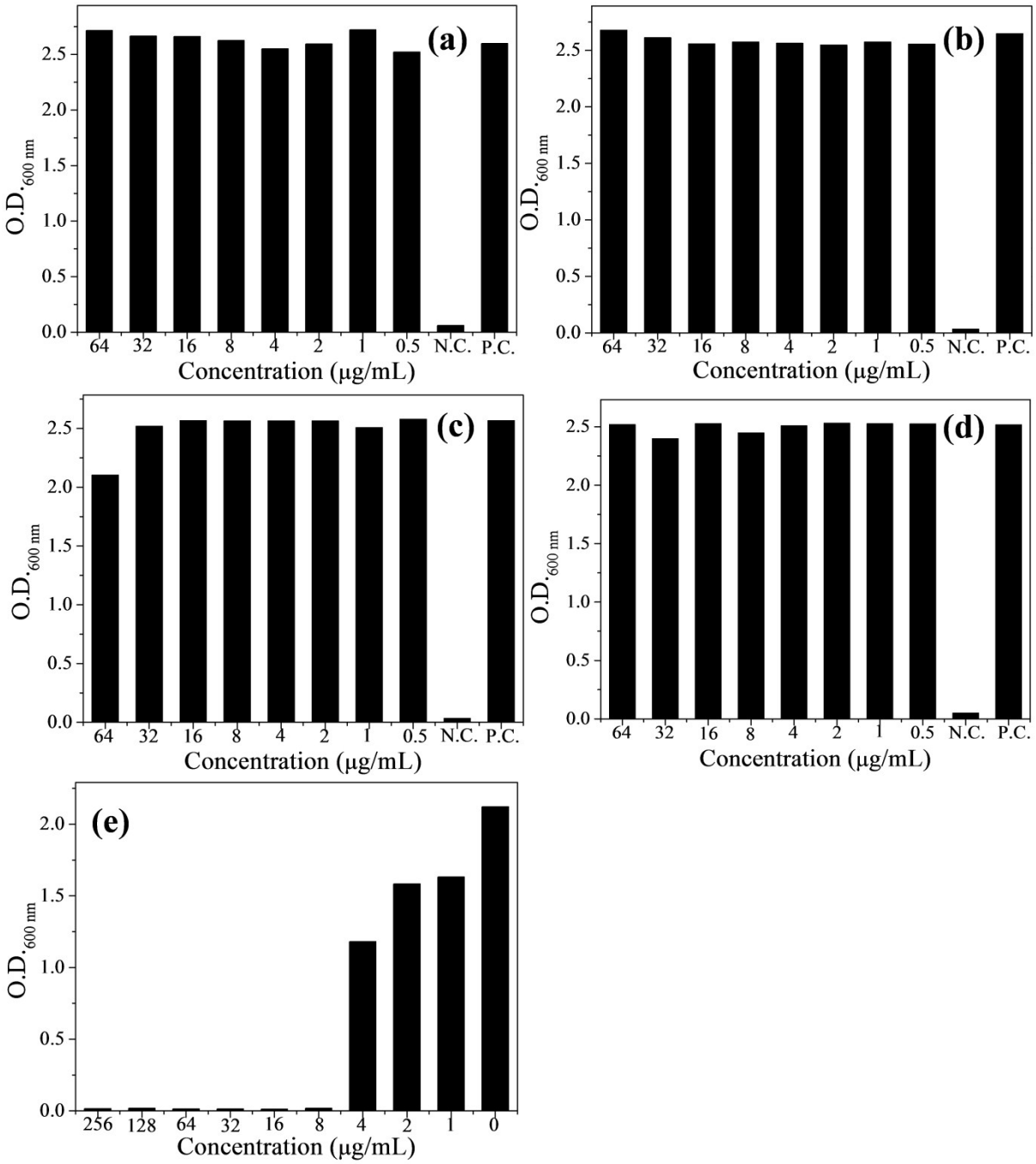

Figure S18. The effect of concentration of (a) control, (b) pH 4 Au NPs, (c) pH 5 Au NPs, (d) pH 6 Au NPs, and (e) CFD antibiotic on the growth of *E. coli*.

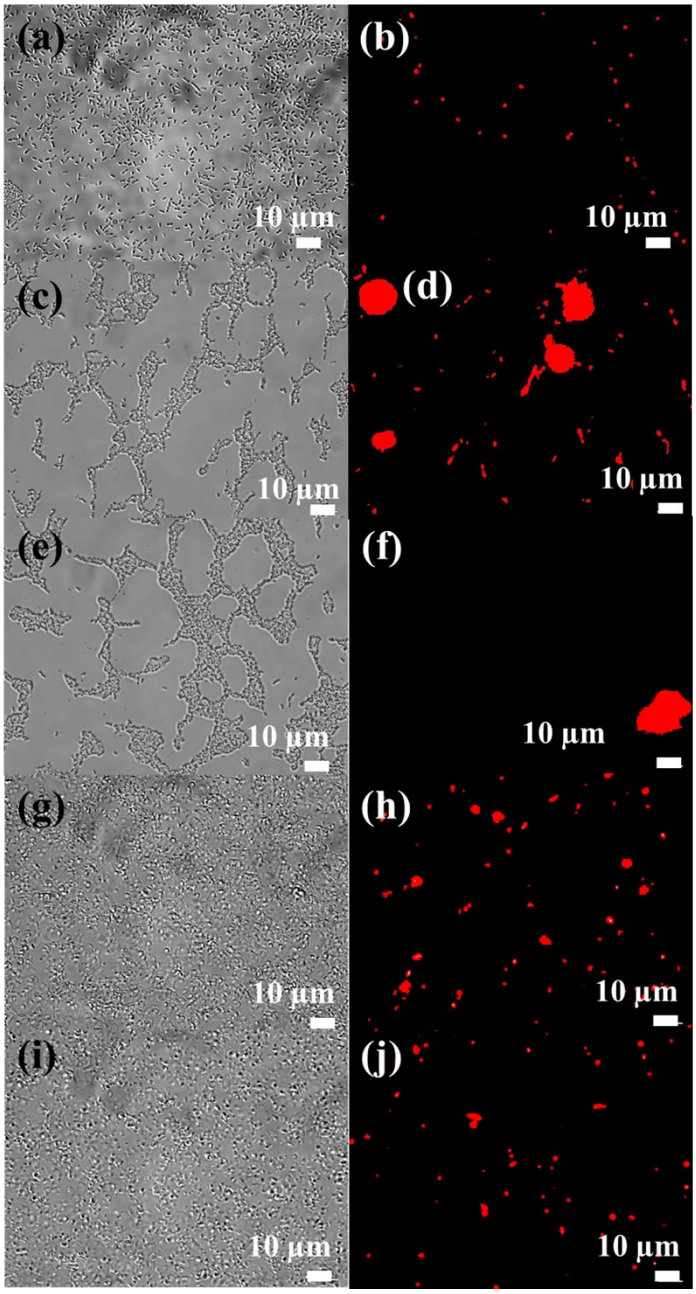

Figure S19. Fluorescence microscopic images of *E. coli* cells after incubation with propidium iodide (a, b) and with both propidium iodide as well as pH 4 Au NPs (c, d), pH 5 Au NPs (e, f), pH 6 Au NPs (g, h), CFD (i, j) in DIC mode (a, c, e, g, i) and fluorescence mode (b, d, f, j, h).

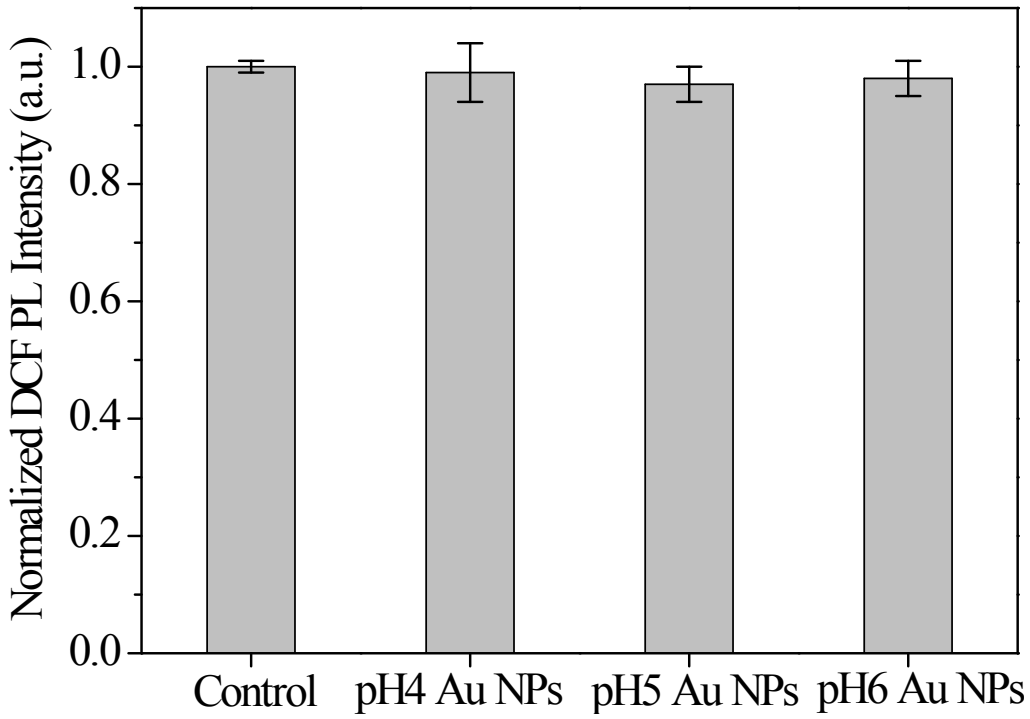

Figure S20. Determination of ROS in NP-treated or untreated *E. coli* using DCF dye. All data are the mean ± standard deviation of triplicate determinations. The ROS assay shows that these Au NPs did not stimulate ROS production and hence, the possibility of ROS to be a mechanism behind loss of cell viability was ruled out in our study.

Table S2. Summary of Mass assignments for observed mass peak. Most probable mass composition is shown in bold and highlighted.

Experimental mass	*a*	*b*	*c*	Calculated mass	Molecular formula $\{Au_a(CFD)_bS_c\}$
2466.6	5	3	13	2449.9	$[Au_5(CFD)_3S_{13}]$
	5	4	2	2446.6	$[Au_5(CFD)_4S_2]$
	5	4	3	2478.6	$[Au_5(CFD)_4S_3]$
	5	5	0	2731.8	$[Au_5(CFD)_5]$
	6	2	0	1880.6	$[Au_6(CFD)_2]$
	6	3	7	2454.4	$[Au_6(CFD)_3S_7]$
	6	3	8	2486.5	$[Au_6(CFD)_3S_8]$
	6	4	0	2579.4	$[Au_6(CFD)_4]$
	7	2	0	2077.6	$[Au_7(CFD)_2]$
	7	3	1	2461	$[Au_7(CFD)_3S]$
	7	3	2	2491.1	$[Au_7(CFD)_3S_2]$
	7	4	0	2776.4	$[Au_7(CFD)_4]$
	8	1	0	1925.1	$[Au_8(CFD)\ ]$
	8	**2**	**6**	**2466.9**	**$[Au_8(CFD)_2S_6]$**
	8	3	0	2623.9	$[Au_8(CFD)_3]$
	9	1	0	2122.1	$[Au_9(CFD)]$
	9	1	10	2442.7	$[Au_9(CFD)S_{10}]$
	9	1	11	2474.8	$[Au_9(CFD)S_{11}]$

	9	2	0	2471.5	$[Au_9(CFD)_2]$
	10	1	4	2447.3	$[Au_{10}(CFD)S_4]$
	10	2	0	2668.5	$[Au_{10}(CFD)_2]$